Electronic Supplementary Information

In Situ Growth of Fe(II)-MOF-74 Nanoarrays on Nickel Foam as Efficient Electrocatalytic Electrode for Water Oxidation: A Mechanism Study on Valence Engineering

Qijun Wang,[a,1] Feifei Wei,[b,1] Devaraj Manoj,[a,1] Zheye Zhang,[a] Junwu Xiao,[a] Xuezhu Zhao,[b] Fei Xiao,[a] Hairen Wang,[b] and Shuai Wang[a*]

[a] School of Chemistry and Chemical Engineering, Huazhong University of Science & Technology, Wuhan, 430074, P. R. China.

[b] School of Materials Science and Engineering, Hubei University, Wuhan, 430062, P. R. China.

[1] These authors contributed equally.

* Corresponding Authors. E-mail addresses: chmsamuel@mail.hust.edu.cn   (S. Wang).

Methods

Materials

Iron (II) chloride tetrahydrate (FeCl$_2$, *J&K* Scientific Ltd.,), Iron (III) chloride tetrahydrate (FeCl$_3$, *J&K* Scientific Ltd.,) N,N-dimethylformamide (DMF, *J&K* Scientific Ltd.,), absolute ethanol (Sinopharam Chemical) and potassium hydroxide (KOH, Sinopharam Chemical) were all of analytical grade without further purification. The 2, 5-dihydroxyterephthalic acid (DHTA), Nafion and iridium (IV) dioxide (IrO$_2$) were purchased from Sigma-Aldrich. The deionized water performed in all experiments, which was fabricated by mini Q, an ultra-pure purification machine. In addition, nickel foam (1 cm × 2.5 cm) was treated by 3 mol/L HCl aqua-solution at 60 ℃ for 30 mins (remove the surface NiO), then successively washed with deionized water, acetone, absolute ethanol, respectively and finally dry in the air.

Preparation of Fe(II), Fe(III)-MOF-74 NAs@NF and Fe(II), Fe(III)-MOF-74 @NF-air

The Ni foams were sonicated in HCl solution (3 M) for 30 min to remove the nickel oxide layer on the surface, rinsed with ultrapure water and absolute ethanol, and then left to dry in air. 1.97 mmol FeCl$_2$ (or FeCl$_3$) and 0.3 mmol 2,5-dihydroxytelephthalic acid were dissolved in 20 mL N, N-dimethyl-formamide (DMF). 1.5 mL ethanol and 1.5 mL H$_2$O were then added to obtain a well dispersed suspension after ultrasonic vibration for 10 min. The resultant solution was then transferred into a 25 mL Teflon-lined stainless steel autoclave. The refreshed Ni foams were vertically immersed into the as-prepared solution and the autoclave was then sealed under argon atmosphere (in the glove box) and placed in an oven (filled with argon atmosphere but not vacuum) at 120 ℃ for 24 h. After that, the autoclave cooled down in the ambient environments. The resultant product was rinsed with ethanol and dried under argon atmosphere. For comparison, the synthesis of Fe(II) and Fe(III)-MOF-74@NF-air

was also synthesized under similar experimental conditions adopted for Fe-MOF-74 NAs@NF without inert atmosphere reaction system. The synthesis of bulk Fe(II)/Fe(III)-MOF-74 is similar to that of Fe(II)/Fe(III)-MOF-74 NAs@NF without using NF substrate.

Materials Characterization

Infrared spectra were recorded by a Bruker VERTEX 70v FT-IR spectrometer in the range of 500-4000 cm^{-1}. Room temperature Raman spectroscopy (Raman) measurement was performed on the inVia-ReflexinVia-Reflex (Renishaw). X-ray diffraction (XRD) was collected on X'pert3 powder (PANalytical B.V.) with Cu Kα radiation (λ = 1.5406 Å) in a 2θ range of 5-80°, the scan rate is 0.08º s^{-1}. The scanning electron microscopy (SEM) was performed on VEGA 3 SBH to observe the morphologies (accelerate voltage: 20 kV). The transmission electron microscopy (TEM) was using FEI Tecnai G2 F30 (accelerate voltage of 200 kV). The X-ray photoelectron spectroscopy (XPS) was performed on AXIS-ULTRA DLD-600W spectrometer. Binding energies (BE) were determined using the C 1s peak at 284.5 eV as a charge reference. Electron paramagnetic resonance (EPR) experiments were performed on the EMXmicro-6/1/P/L spectrometer (X-band at 9.8 GHz, power of 2 mW).
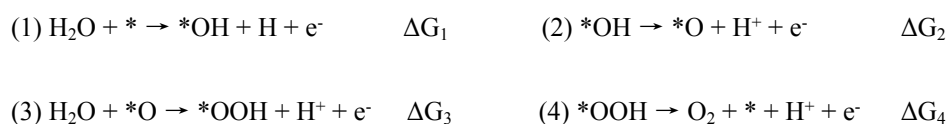
Electrochemical measurements

In this part, all measurements were performed by using CHI 760E electrochemistry workstation. Using Fe-MOF-74 NAs@NF as the working electrode, the carbon rod as the counter electrode and the reference electrode is Hg/HgO electrode to form the standard three-electrode system. All potentials measured were calibrated to RHE through Nernst equation: E(RHE) = E(Hg/HgO) + 0.098 + 0.059 × pH (in 1.0 M KOH). 1.0 M KOH electrolyte was treated by oxygen (for OER) bubbles before the test. Moreover, the polarization curves were obtained using LSV for OER in 1.0 M KOH with a scan rate of 1 mV s^{-1}, respectively. i*R* drop was set at 95% for OER. All potentials are transformed to the scale of

the reversible hydrogen electrode (RHE) via calibration (Fig. S8). For comparison, NF and IrO_2 was used as the benchmark catalysts. In a typical prepare method of noble metal benchmark catalyst, we first add 10 mg IrO_2 into the mixture of DMF (490 μL) and Nafion (10 μL), using ultrasonic treatment for 30 mins to gain the dark black mixture solution. Then drop 10 μL of this mixture solution onto the two surfaces of 1×1 nickel foam (cleaned) to form the benchmark electrode after heat stoving by filament lamp. The faradaic efficiency of the catalyst in the OER is defined as the ratio of the amount of O_2, evolved during the experimental test to the amount of O_2 expected based on theoretical calculations. Here, the O_2 generated from the electrocatalysis was collected using the water-drainage method. Then, the moles of O_2 generated from the reaction was obtained with the ideal gas law. The theoretical amount of O_2 was calculated according to the Faraday law.

Computational Section

The density of state calculations for Fe(II)-MOF-74 and Fe(III)-MOF-74 were performed by using CASTEP (one model of Materials Studio 8.0). Both electron exchange along with correlation effects were performed via Perdew-Burker-Ernzerhof (PBE) method and generalized gradient approximation (GGA) type exchange correlation function.[S1-S3] The wave functions at each k-point were expanded with a plane wave basis set and a kinetic cutoff energy up to 400 eV. K-point mesh was set to $1 \times 1 \times 1$ and fermi smearing was adopted during the calculation process. The geometries were optimized until the energy was converged to 2×10^{-6} eV/atom. The following mechanisms are promoted for the OER:

(1) $H_2O + * \rightarrow *OH + H + e^-$ $\quad\quad \Delta G_1$ $\quad\quad$ (2) $*OH \rightarrow *O + H^+ + e^-$ $\quad\quad\quad \Delta G_2$

(3) $H_2O + *O \rightarrow *OOH + H^+ + e^-$ $\quad \Delta G_3$ $\quad\quad$ (4) $*OOH \rightarrow O_2 + * + H^+ + e^-$ $\quad \Delta G_4$

Double-layer capacitance (Cdl):

The double-layer capacitance (Cdl) is proportional to the effective electrochemical surface, which were measured by using cyclic voltammetry method. We measured the currents density in a narrow potential window that no faradic processes were observed at various scan rates (20-100 mV s^{-1}), thus the currents should be due to the charging of the double layer, which is expected to be linearly proportional to the effective surface area of the Fe-MOF-74 NAs@NF catalyst. By plotting the capacitive currents ($\Delta j = j_{anodic} - j_{cathodic}$) against the scan rate and following with a linear fit, the double layer capacitance (Cdl, mF cm^{-2}) can be estimated as the half of the slope.

Note

The synergistic effect of Ni-Fe leads to excellent electrochemical performance, however, because of the interesting synergistic effect of Ni-Fe, this couple has been studied very widely and deeply, especially in pristine MOFs. So that in this study, we choose a different angle of view to enhance the electrocatalytic performance *via* valance engineering. The main idea which we hope to describe in the manuscript was the valence influence of Fe on electrochemical performance, especially Fe^{2+}, not the synergistic effect of Ni-Fe, so we constructed an inert atmosphere reaction system to engineer the valence of Fe. In our proposed system, the oxidation reaction of Fe^{2+} cannot happened during the synthesis process of Fe(II)-MOF-74 NAs@NF (because there're precious few of oxygen), so that Ni-Fe couple may not exist in the as synthesized Fe(II)-MOF-74 NAs@NF. As we know, the reaction of $2Fe^{3+} + Ni = 2Fe^{2+} + Ni^{2+}$ is spontaneous, however, this reaction will not be activated during the synthesis of Fe(II)-MOF-74 NAs@NF. The oxidation of Fe^{2+} was a chain-reaction, which contain two steps: the first step is: $4Fe^{2+} + O_2 + H_2O = 4Fe^{3+} + 4OH^-$, and then the step ii can be activated by the as formed Fe^{3+}: $2Fe^{3+} + Ni = 2Fe^{2+} + Ni^{2+}$, which means that without the step i during the synthesis of Fe(II)-MOF-74 NAs@NF, the step ii ($2Fe^{3+} + Ni = 2Fe^{2+} + Ni^{2+}$) cannot be activated. These two steps

can be described as follow: Firstly, if much oxygen came into our reaction system during the synthesis process, the Fe^{2+} ions in our system will be soon oxidized to Fe^{3+}. Then, the Fe^{3+} ions will etch the nickel foam to obtain Fe^{2+} ions. Finally, the Fe^{2+} ions will be oxidized by oxygen again to form Fe^{3+} ions to keep the reaction balance. However, our careful experiment under inert atmosphere can avoid this chain-reaction. Even precious few of oxygen came into our careful constructed inert atmosphere system, a very few of Fe^{2+} may be oxidized to Fe^{3+}, nevertheless, at the ending of the reaction, the as formed few Fe^{3+} ions will be reduced to Fe^{2+} by Ni, thus the Fe^{3+} ions will not exist in the as synthesized Fe(II)-MOF-74 NAs@NF, which can engineer the valence of iron and embody the primary and significant role of Fe^{2+} ions.
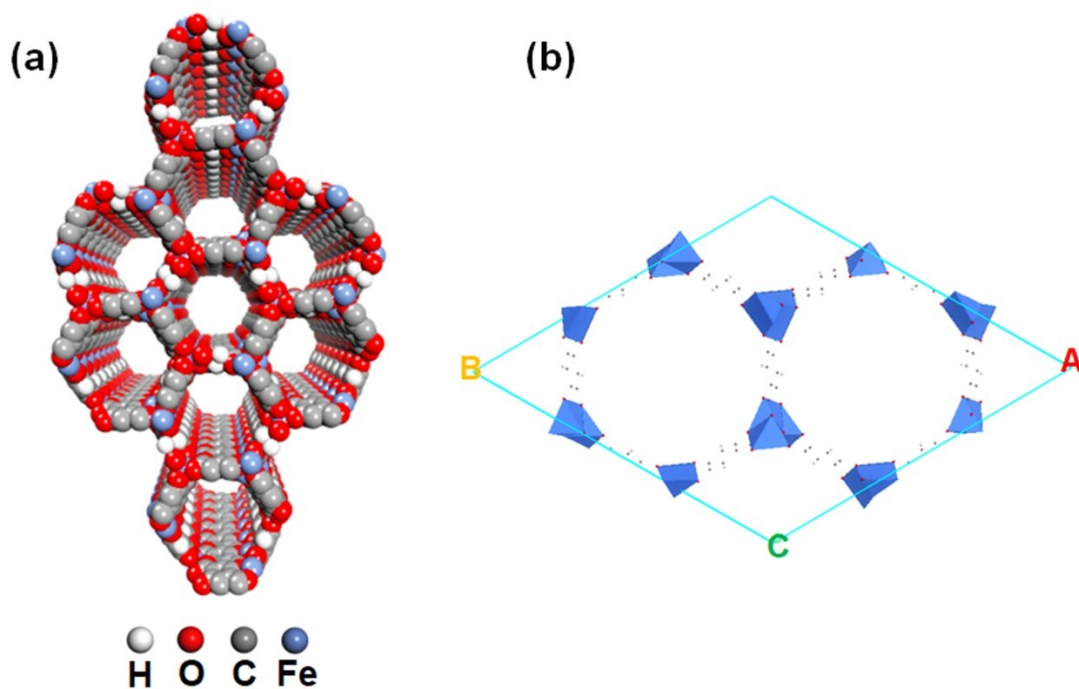
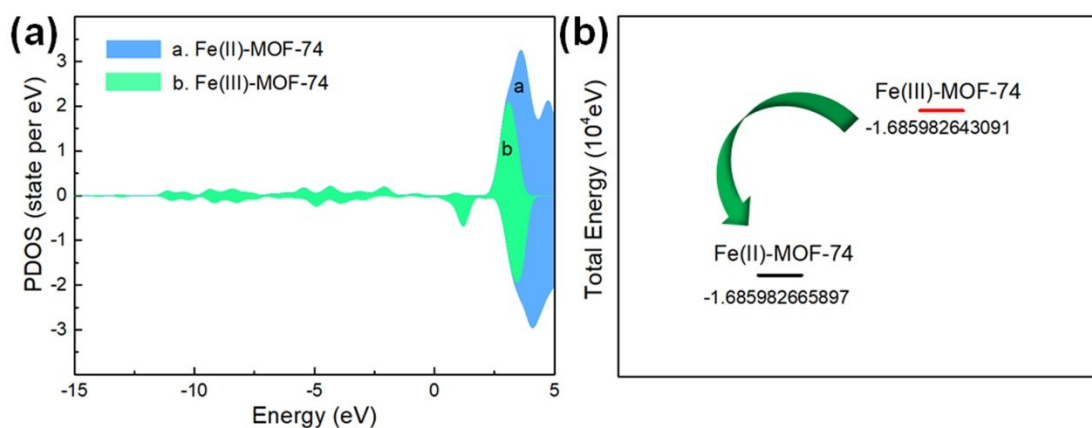**Fig. S1** Stacking view (left) and polyhedral view (right) of the Fe-MOF-74 model.

Fig. S2 Comparison of Fe(II)-MOF-74 and Fe(III)-MOF-74. (a) Partial density of states (PDOS) of the

p orbital of Fe. (b) Total energy.

Note

In our study, it was found that the PDOS area of the discrete 2p-orbital of Fe in Fe(II)-MOF-74 is

larger than that of Fe(III)-MOF-74 (Fig. S2a), which indicate the Fe(II)-MOF-74 own better electronic

conductivity. In addition, the total energy of Fe(II)-MOF-74 is much lower than Fe(III)-MOF-74 (Fig.

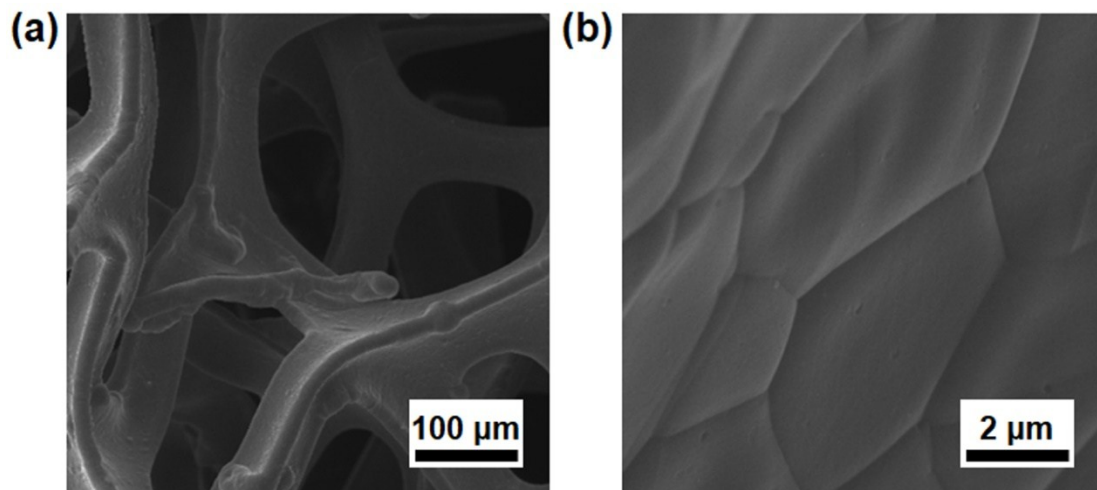S2b), suggesting the Fe-MOF-74 in low valence Fe^{2+} own better stability than high valence Fe^{3+}.

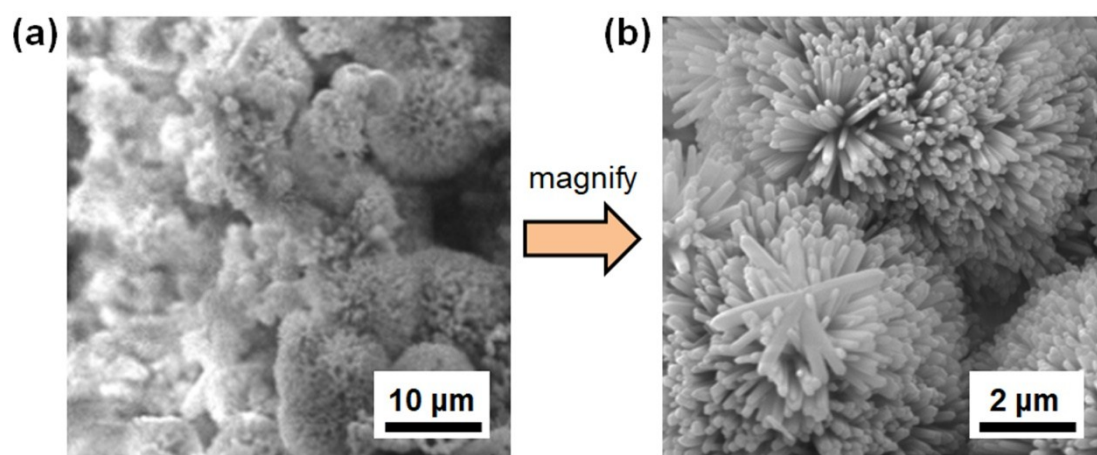**Fig. S3** SEM images of the nickel foam after HCl treatment.

Fig. S4 SEM images of the Fe(II)-MOF-74 (DMF: 20 mL, ethanol: 1.2 mL, H_2O: 1.2 mL).
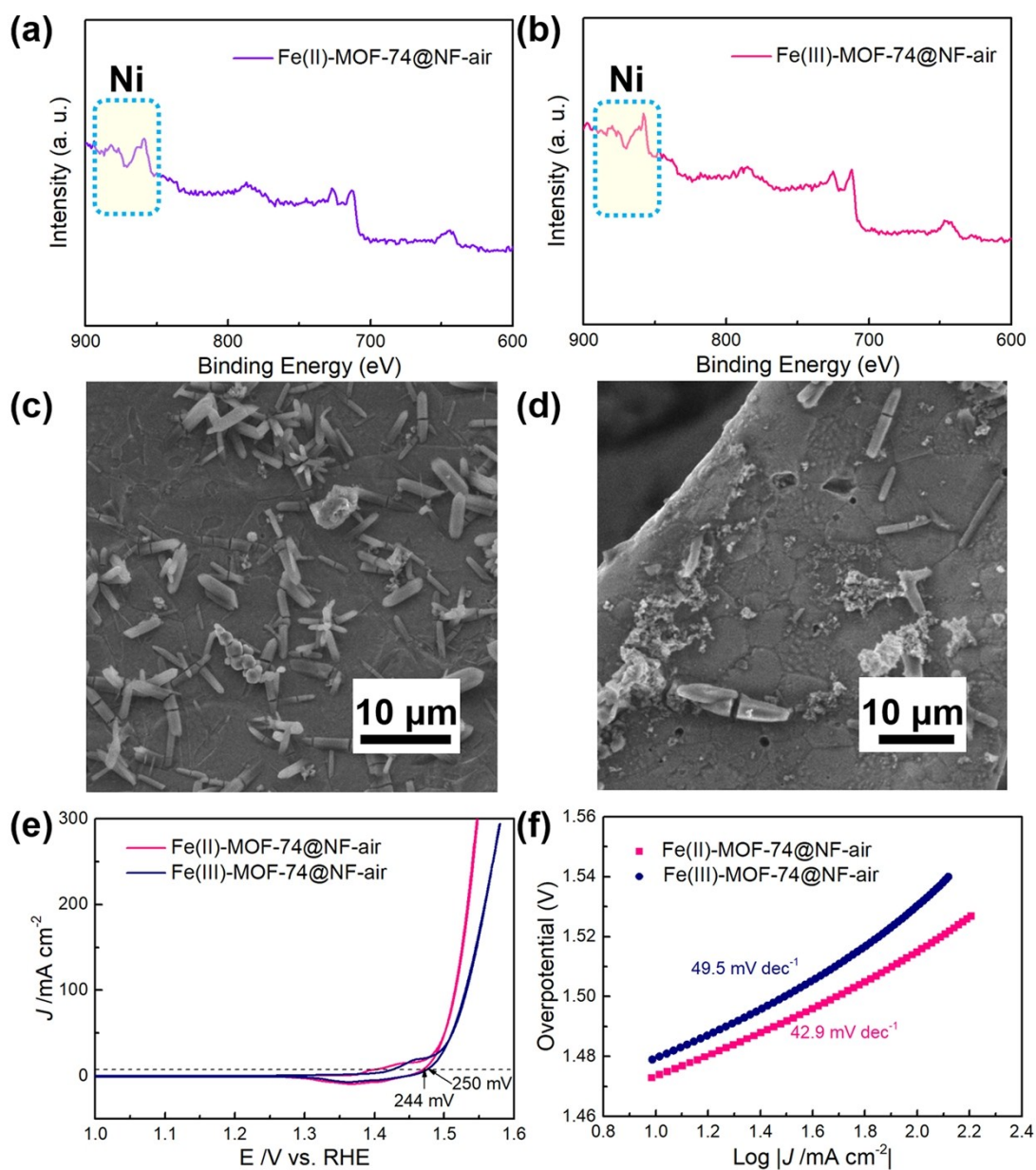
Fig. S5 (a, b) XPS spectra, (c, d) SEM images and (e, f) OER performance of the as synthesized Fe(II)-MOF-74@NF-air and Fe(III)-MOF-74@NF-air, respectively.

Note for in situ growth of nanoarrays on nickel foam

After our careful experimental condition under argon atmosphere, the hydrothermal in situ growth of Fe(II)-MOF-74 on nickel foam with uniform nanoarray structure may depends on the ratio of ethanol and H_2O. As shown in Fig. S4, tuning the ratio of ethanol and H_2O from 1.5 mL to 1.2 mL, the structure of Fe(II)-MOF-74 was changing from uniform nanoarrays to delicate clusters. In addition, as

illustrated in Fig. S5a and S5b, the typical Ni peaks of XPS survey spectra of Fe(II)-MOF-74@NF-air and Fe(III)-MOF-74@NF-air were observed. This phenomenon indicates that with the influence of oxygen in air atmosphere, the Fe^{2+} ions were oxidized to Fe^{3+} which can etch the nickel foam to release the nickel ions. Moreover, the Ni ions may combine with Fe ions to form the Ni-Fe, a widely discussed synergetic couple for electrocatalysis, thus cannot embody the primary and significant role of Fe^{2+} for OER electrocatalysis in this study. Furthermore, the SEM images of Fe(II) and Fe(III)-MOF-74@NF-air were shown in Fig. S5c-S5d. These morphology images indicated that the uniform nanoarrays cannot be synthesized in air. Furthermore, Fe(II) and Fe(III)-MOF-74@NF-air as electrocatalysts were subjected to OER test in 1.0 M KOH (Fig. S5e, S5f). The as synthesized Fe(II) and Fe(III)-MOF-74@NF-air electrode possesses the catalytic activity with overpotential of 244 and 250 mV to achieve the current density of 10 mA cm^{-2}, respectively. The Tafel slope of Fe(II) and Fe(III)-MOF-74@NF-air are 42.9 and 49.5 mV dec^{-1}, which were worse than that of Fe(II)-MOF-74 NAs@NF. The above results of our control experiments clearly demonstrate that the inert atmosphere play an important role in the proposed synthesis route.
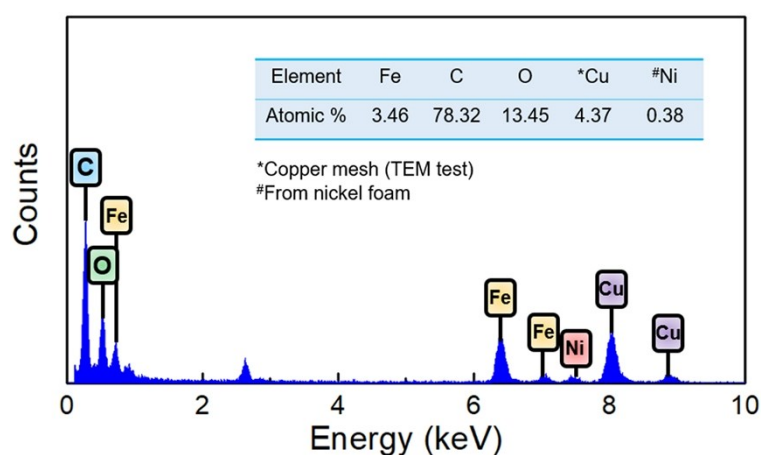

Element	Fe	C	O	*Cu	#Ni
Atomic %	3.46	78.32	13.45	4.37	0.38

*Copper mesh (TEM test)
#From nickel foam

Fig. S6 EDS spectrum of the Fe(II)-MOF-74 (removed from the nickel foam by the continuous ultrasound in EtOH)
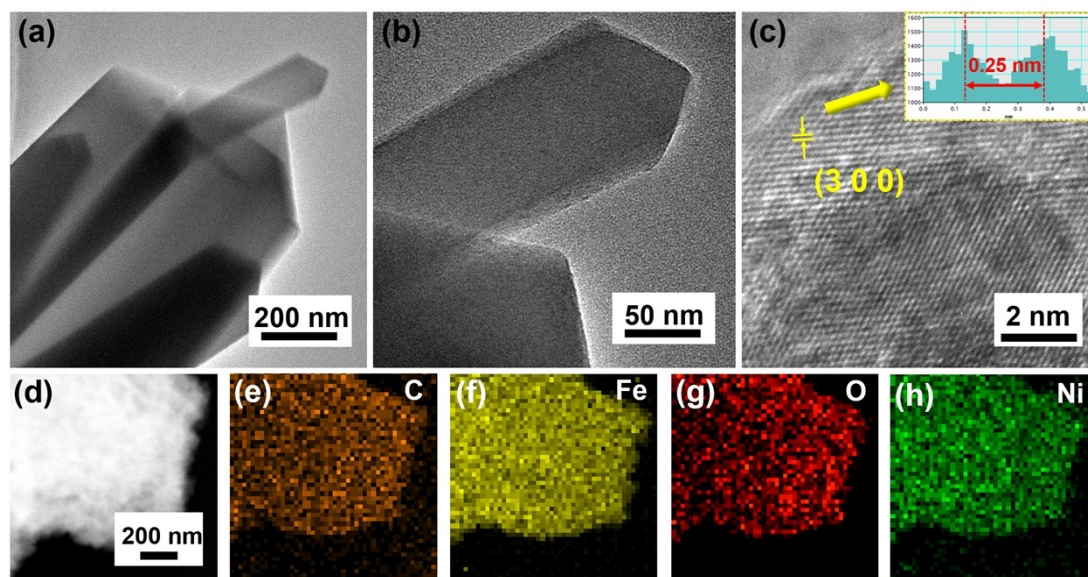
Fig. S7 (a, b) TEM image of Fe(III)-MOF-74. (c) HRTEM image of Fe(III)-MOF-74 and the intensity profiles of the d-spacing of the (3 0 0) crystal phase (inset pattern). STEM pattern (d) and the corresponding elemental mapping images ((e) C, orange, (f) Fe, yellow, (g) O, red, (h) Ni, green) of Fe(III)-MOF-74.
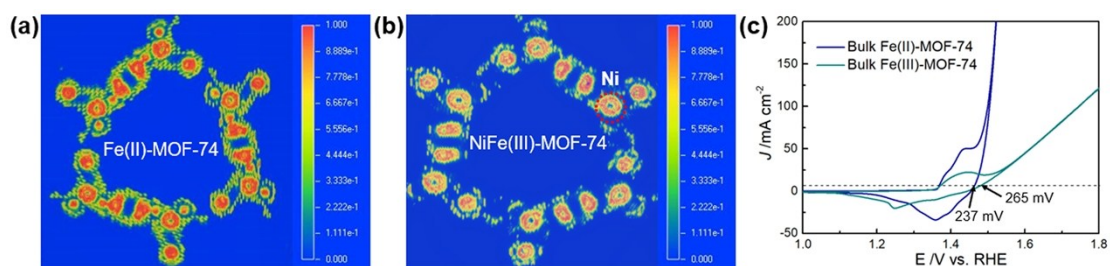

Fig. S8 ELF mapping patterns for (a) Fe(II)-MOF-74 and (b) NiFe(III)-MOF-74. (c) OER performance of the as synthesized Bulk Fe(II)-MOF-74 and Bulk Fe(III)-MOF-74, respectively.

Note

According to the Fig. S7, the as synthesized Fe(III)-MOF-74 contain some Ni element. In order to remove the influence of Ni, on the one hand, we have added the electron localization function (ELF) mapping of NiFe(III)-MOF-74 (Fig. S8a and S8b). The results show that with the same scale bar, the electron distribution in NiFe(III)-MOF-74 was found to be still lower than Fe(II)-MOF-74. So that the

influence of Ni ions etch from nickel foam by Fe^{3+} is inconsequential and doesn't affect the conclusion and the efficient performance of Fe(II)-MOF-74 in this work. On the other hand, although the nickel foam is the suitable substrate for the in situ growth of Fe-MOF-74 nanoarrays, but in order to remove the effect of Ni in our careful designed experimental system, we have synthesized Fe(II) and Fe(III)-MOF-74 powder and loaded them on nickel foam (Bulk Fe(II)/Fe(III)-MOF-74) as an electrode for OER test (The synthesis of bulk Fe(II)/Fe(III)-MOF-74 is similar to that of Fe(II)/Fe(III)-MOF-74 NAs@NF without using NF substrate). The Fe(II) or Fe(III)-MOF-74 powder (10 mg) was dispersed in the mixture of DMF (490 μL) and Nafion (10 μL), using ultrasonic treatment for 30 mins to gain the dark black mixture solution. Then drop 10 μL of this mixture solution onto the two surfaces of 1×1 nickel foam (cleaned) to form the benchmark electrode after heat stoving by filament lamp. As shown in Fig. S8c, the OER performance of Bulk Fe(III)-MOF-74 was still worse than that of Bulk Fe(II)-MOF-74, while both Bulk Fe(II) and Fe(III)-MOF-74 were worse than the Fe(II)-MOF-74 NAs@NF. The results directly demonstrate that both valence engineering and nickel foam play an important role as efficient method/substrate to fabricate high performance pristine MOF nanoarrays for electrochemical water oxidation.
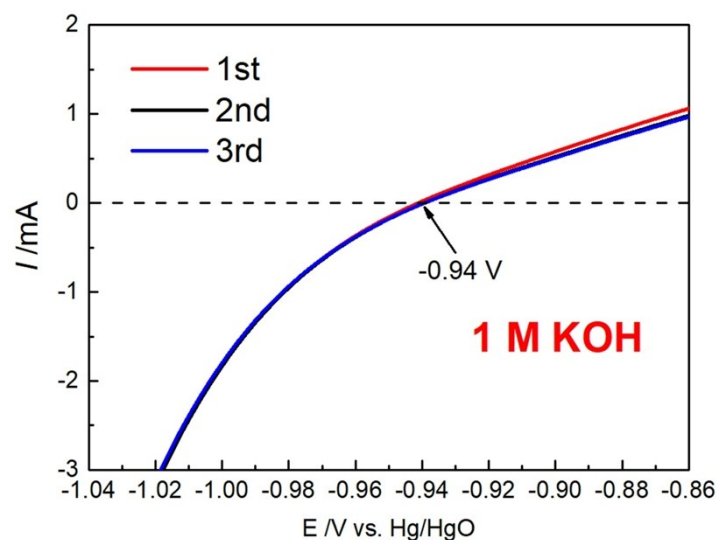
Fig. S9 The typical calibration of Hg/HgO reference electrode with respect to RHE in 1M KOH.
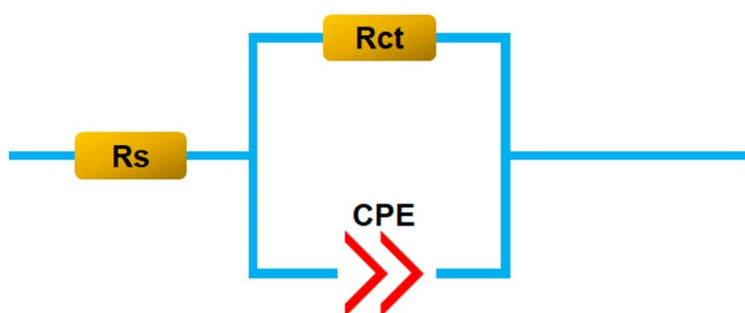

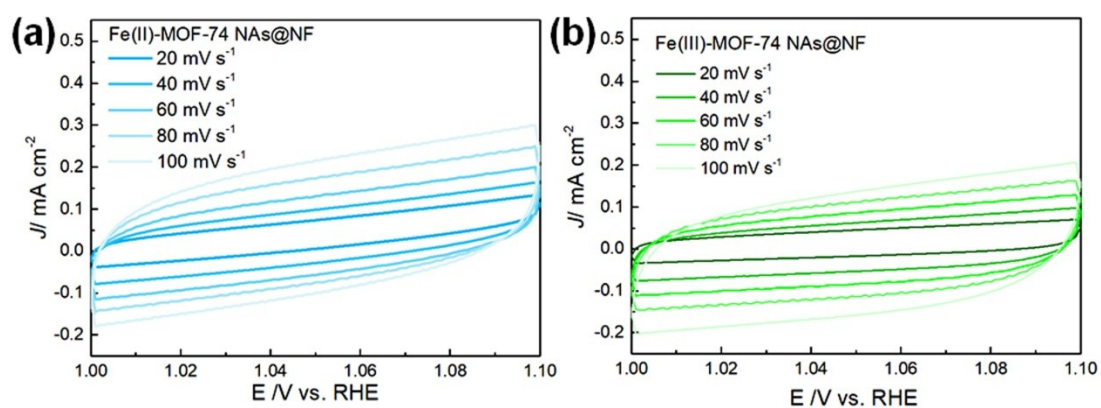**Fig. S10** Equivalent circuit diagram of the electrochemical double-layer capacitance measurements.

Fig. S11 Electrochemical double-layer capacitances of the (a) Fe(II)-MOF-74 NAs@NF and (b) Fe(III)-MOF-74 NAs@NF, respectively.
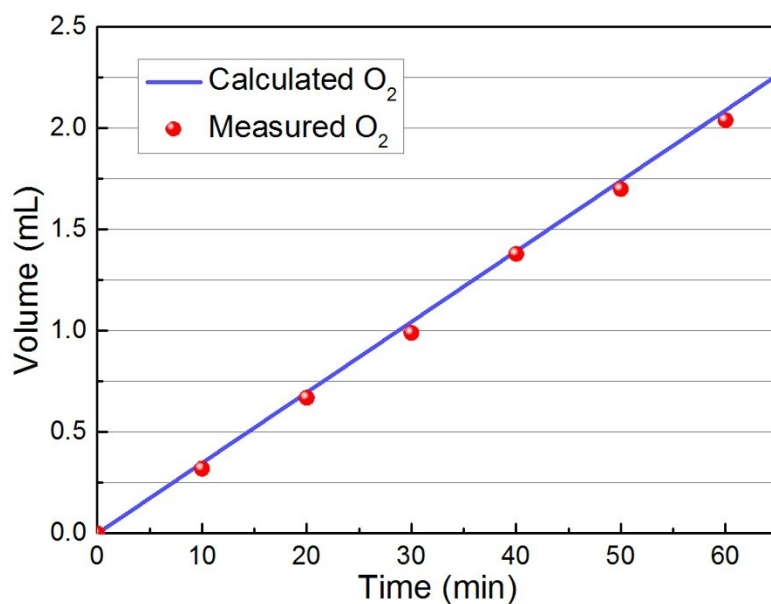
Fig. S12 The volume of oxygen theoretically calculated and experimentally measured versus time for Fe(II)-MOF-74 NAs@NF.
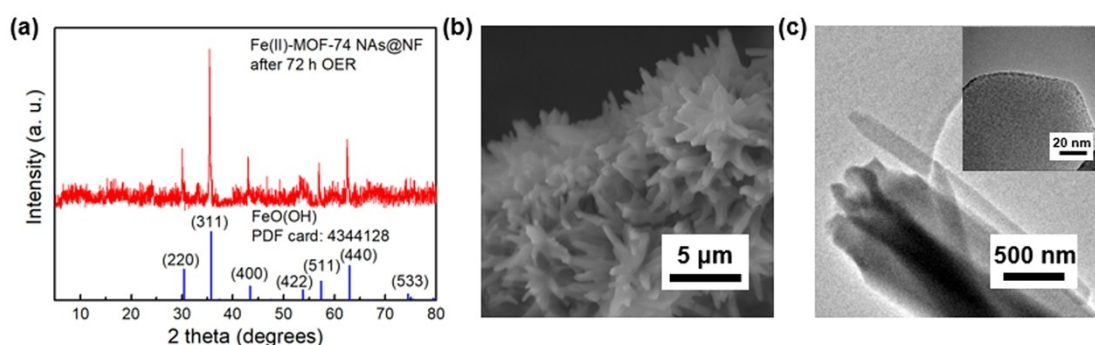
Fig. S13 (a) XRD pattern, (b) SEM and (c) TEM image of Fe(II)-MOF-74 NAs@NF after 72 h OER.

Note

As shown in Fig. S12a, the XRD pattern of Fe(II)-MOF-74 NAs@NF after 72 h OER agrees well with that of FeO(OH) (PDF card number: 4344128), which demonstrates the formation of hydroxides and the results further verified the consequence of XPS results (Fig. S14). The SEM and TEM images (Fig. S12b and S12c) indicate that the as synthesized Fe(II)-MOF-74 NAs@NF can remain its nanoarray and prism morphology after 72 h OER, which further demonstrates its excellent long-term stability.
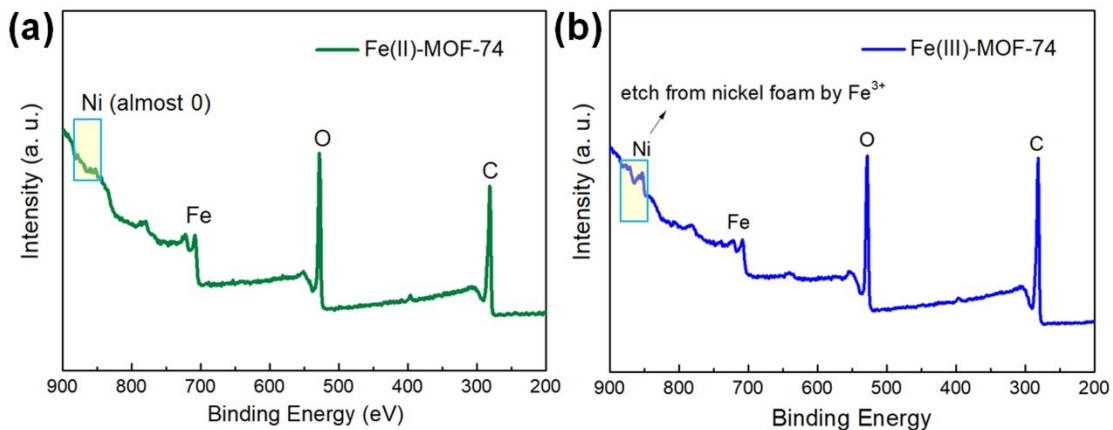
Fig. S14 XPS survey spectra of the (a) Fe(II)-MOF-74 and (b) Fe(III)-MOF-74, respectively.
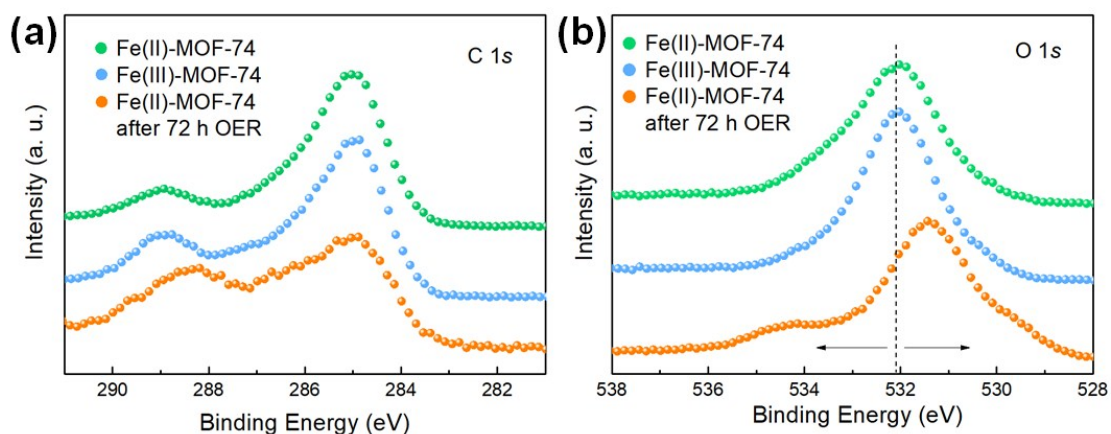
Fig. S15 XPS high-resolution spectra of (a) C 1s and (b) O 1s for Fe(II)-MOF-74, Fe(III)-MOF-74 and Fe(II)-MOF-74 after 72h chronoamperometric test.

Note

As shown in Fig. S14, after 72 h chronoamperometric test, the XPS results indicate that the C 1s spectra have no obvious difference, while the O 1s spectra is different from the others. In Fe(II)-MOF-74 (after 72 h OER), the peak near 531 eV can be ascribed to the metal–O–H, which demonstrates the formation of hydroxides. Notably, these as formed hydroxides can act as important species to enhance the OER activity.[S4-S6]
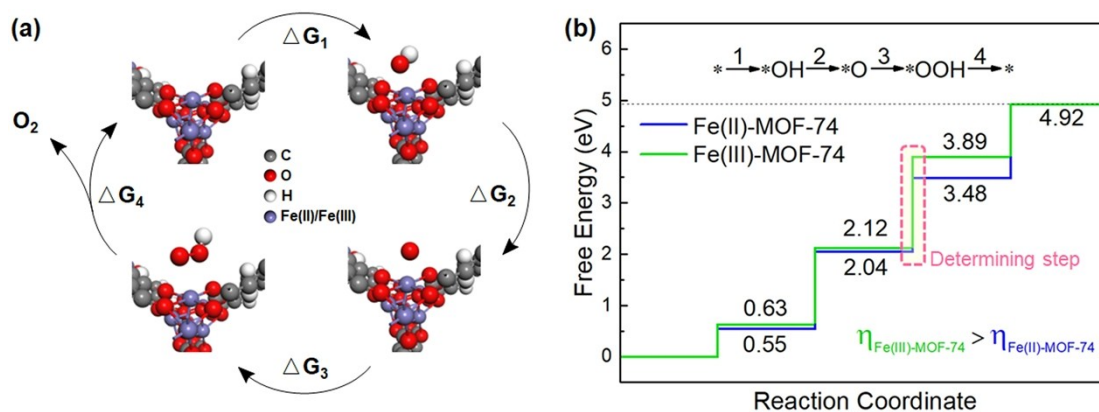
Fig. S16 (a) Simulated model and adsorption geometries. Top-left, substrate; top-right, adsorbed OH; bottom-right, adsorbed O; bottom-left, adsorbed OOH. (b) Gibbs free energy landscape for the four steps of OER on Fe(II)-MOF-74 (blue line) and Fe(III)-MOF-74 (green line).

Note

With the ideal catalyst, the kinetic barriers would be vanishingly small, and all four reaction steps would be equal, requiring the application of an external potential of (4.92 eV)/4e = 1.23 V. The overpotential η is defined in Equation:

$\eta = \max(\Delta G_1, \Delta G_2, \Delta G_1, \Delta G_4)/e - 1.23$ eV

Fig. S17 EPR data for Fe(II)-MOF-74, Fe(III)-MOF-74 and Fe(II)-MOF-74 after 72 h OER process.

Table S1. Overpotential and Tafel slope of the reported Fe contained nonprecious metal electrocatalysts and MOFs as electrocatalysts for OER (J: current density; η: overpotential at $J = 10$ mA cm^{-2})

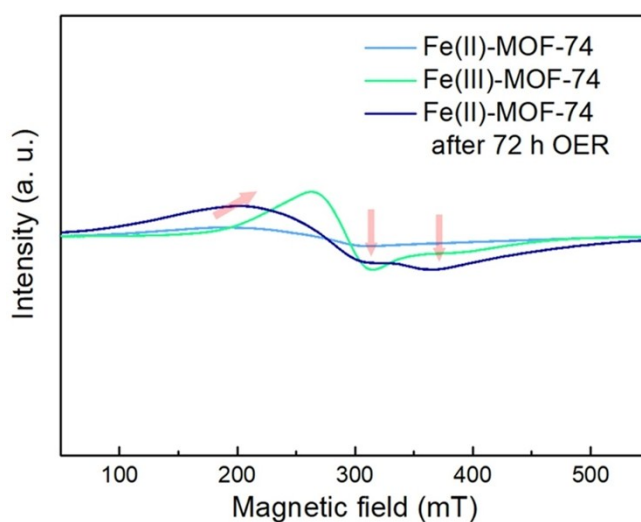| Catalyst	Electrolyte	η(mV)	Tafel Slope (mV/dec)	Reference
Fe(II)-MOF-74 NAs@NF	1 M KOH	207	41.1	This work
Fe(III)-MOF-74 NAs@NF	1 M KOH	220	44.5	This work
CoFe-MOF-74	1 M KOH	280	56	*ACS Energy Lett*. 2018, 310, 2520-2526
NiFe-LDH NPs	1 M KOH	230	50	*Chem. Commun*. 2014, 50, 6479-6482
NiFe LDH/CNT	1 M KOH	240	43	*J. Am. Chem. Soc.* 2013, 135, 8452-8455
NiFe-MOF-74	1 M KOH	223	76	*Chem. Commun.* 2018, 54, 7046--7049
Fe/Ni-BTC@NF	1 M KOH	270	47	*ACS Appl. Mater. Interfaces* 2016, 8, 16736-16743
NiFe-UMNs	1 M KOH	260	30	*Nano energy* 2018, 44, 345-352
NiFe-MOF nanosheets	1 M KOH	240	-	*Nat. Commun.* 2017,8,15341-15348
FeNi$_3$N/NF	1 M KOH	202	40	*Chem. Mater.* 2016, 28, 6934-6941
FeCo-Co$_4$N/N-C	1 M KOH	280	40	*Adv. Mater.* 2017, 29, 1704091.
Co-Fe-N@MWCNT	1 M KOH	290	32	*Electrochim. Acta* 2017, 258, 51-60
CoyFe$_{10-y}$O$_x$/NPC	1 M KOH	328	31.4	*J. Mater. Chem. A* 2016, 4, 6505-6512
CoFe$_2$O$_4$/PANI-MWCNT$_{1:20}$	1 M KOH	314	30.69	*J. Mater. Chem. A* 2016, 4, 4472-4478.
Fe-CoOOH/G	1 M KOH	330	37	*Adv. Energy. Mater.* 2017, 7, 1602148

Table S2. Fractional coordinates of atoms in the model of Fe(II)-MOF-74.

Atom	Fractional coordinates of atoms		
	U	V	W
H	1.153978	0.697563	0.129416
H	0.129416	1.153978	0.697563
H	0.697563	0.129416	1.153978
H	-1.15398	-0.69756	-0.12942
H	-0.12942	-1.15398	-0.69756
H	-0.69756	-0.12942	-1.15398
C	1.137077	0.736323	0.305072
C	1.326261	0.87394	0.411289
C	1.473901	0.951052	0.373479
C	1.306744	0.831207	0.292804
C	0.305072	1.137077	0.736323
C	0.411289	1.326261	0.87394
C	0.373479	1.473901	0.951052
C	0.292804	1.306744	0.831207
C	0.736323	0.305072	1.137077
C	0.87394	0.411289	1.326261
C	0.951052	0.373479	1.473901
C	0.831207	0.292804	1.306744
C	-1.13708	-0.73632	-0.30507
C	-1.32626	-0.87394	-0.41129
C	-1.4739	-0.95105	-0.37348
C	-1.30674	-0.83121	-0.2928
C	-0.30507	-1.13708	-0.73632
C	-0.41129	-1.32626	-0.87394
C	-0.37348	-1.4739	-0.95105
C	-0.2928	-1.30674	-0.83121
C	-0.73632	-0.30507	-1.13708
C	-0.87394	-0.41129	-1.32626
C	-0.95105	-0.37348	-1.4739
C	-0.83121	-0.2928	-1.30674
O	0.959536	0.573615	0.110053
O	1.156931	0.78772	0.418934
O	1.432508	0.891198	0.240505
O	0.110053	0.959536	0.573615
O	0.418934	1.156931	0.78772
O	0.240505	1.432508	0.891198
O	0.573615	0.110053	0.959536

O	0.78772	0.418934	1.156931
O	0.891198	0.240505	1.432508
O	-0.95954	-0.57362	-0.11005
O	-1.15693	-0.78772	-0.41893
O	-1.43251	-0.8912	-0.24051
O	-0.11005	-0.95954	-0.57362
O	-0.41893	-1.15693	-0.78772
O	-0.24051	-1.43251	-0.8912
O	-0.57362	-0.11005	-0.95954
O	-0.78772	-0.41893	-1.15693
O	-0.8912	-0.24051	-1.43251
Fe	1.302076	0.634755	0.036934
Fe	0.036934	1.302076	0.634755
Fe	0.634755	0.036934	1.302076
Fe	-1.30208	-0.63476	-0.03693
Fe	-0.03693	-1.30208	-0.63476
Fe	-0.63476	-0.03693	-1.30208

Table S3. Fractional coordinates of atoms in the model of Fe(III)-MOF-74.

Atom	Fractional coordinates of atoms		
	U	V	W
H	1.153982	0.697607	0.129453
H	0.129453	1.153982	0.697607
H	0.697607	0.129453	1.153982
H	-1.15398	-0.69761	-0.12945
H	-0.12945	-1.15398	-0.69761
H	-0.69761	-0.12945	-1.15398
C	1.137121	0.736371	0.305156
C	1.32627	0.873925	0.411307
C	1.473879	0.951044	0.37346
C	1.306741	0.831219	0.292821
C	0.305156	1.137121	0.736371
C	0.411307	1.32627	0.873925
C	0.37346	1.473879	0.951044
C	0.292821	1.306741	0.831219
C	0.736371	0.305156	1.137121
C	0.873925	0.411307	1.32627
C	0.951044	0.37346	1.473879
C	0.831219	0.292821	1.306741
C	-1.13712	-0.73637	-0.30516
C	-1.32627	-0.87393	-0.41131
C	-1.47388	-0.95104	-0.37346
C	-1.30674	-0.83122	-0.29282
C	-0.30516	-1.13712	-0.73637
C	-0.41131	-1.32627	-0.87393
C	-0.37346	-1.47388	-0.95104
C	-0.29282	-1.30674	-0.83122
C	-0.73637	-0.30516	-1.13712
C	-0.87393	-0.41131	-1.32627
C	-0.95104	-0.37346	-1.47388
C	-0.83122	-0.29282	-1.30674
O	0.9596	0.573682	0.110148
O	1.156951	0.78774	0.418993
O	1.432486	0.891181	0.240484
O	0.110148	0.9596	0.573682
O	0.418993	1.156951	0.78774
O	0.240484	1.432486	0.891181
O	0.573682	0.110148	0.9596
O	0.78774	0.418993	1.156951
O	0.891181	0.240484	1.432486
O	-0.9596	-0.57368	-0.11015

O	-1.15695	-0.78774	-0.41899
O	-1.43249	-0.89118	-0.24048
O	-0.11015	-0.9596	-0.57368
O	-0.41899	-1.15695	-0.78774
O	-0.24048	-1.43249	-0.89118
O	-0.57368	-0.11015	-0.9596
O	-0.78774	-0.41899	-1.15695
O	-0.89118	-0.24048	-1.43249
Fe	1.302103	0.634771	0.036983
Fe	0.036983	1.302103	0.634771
Fe	0.634771	0.036983	1.302103
Fe	-1.3021	-0.63477	-0.03698
Fe	-0.03698	-1.3021	-0.63477
Fe	-0.63477	-0.03698	-1.3021

References

S1, G. Kresse, D. Joubert, *Phys. Rev. B*. 1999, **59**, 1758-1775.

S2 P. E. Blöchl, *Phys. Rev. B*. 1994, **50**, 17953-17979.

S3 J. P. Perdew, K. Burke, M. Ernzerhof, *Phys. Rev. Lett*. 1996, **77**, 3865-3868.

S4 S. Jin, *ACS Energy Lett.* 2017, **2**, 1937-1938.

S5 P. Sennu, V. Aravindan, Y. S. Lee, *J. Power Sources*. 2016, **306**, 248-257.

S6 J. Zhao, Z. J. Li, M. Zhang, A. Meng, Q. D. Li, *ACS Sustainable Chem. Eng*. 2016, **4**, 3598-3608.